ELSEVIER

Journal of Volcanology and Geothermal Research 105 (2001) 183–206

Journal of volcanology and geothermal research

www.elsevier.nl/locate/jvolgeores

Geodetic and seismic constraints on recent activity at Long Valley Caldera, California: evidence for viscoelastic rheology

A.V. Newman[a], T.H. Dixon[b,*], G.I. Ofoegbu[c], J.E. Dixon[b]

[a]*Department of Geological Sciences, Northwestern University, 1847 Sheridan Road, Evanston, IL 60208, USA*
[b]*Rosenstiel School of Marine and Atmospheric Science, University of Miami, 4600 Rickenbacker Causeway, Miami, FL 33149, USA*
[c]*Southwest Research Institute, 6220 Culebra Road, San Antonio, TX 78228-0510, USA*

Received 5 November 1998; accepted 20 August 2000

Abstract

Long Valley Caldera is an active volcanic region in east central California. Surface deformation on the resurgent dome within the caldera was an order of magnitude higher for the five-month period September 1997 through January 1998 compared to the previous three-year average. However, the location of the immediate (shallow) source of deformation remained essentially constant, 5–7 km beneath the dome, near the top of a region of probable magma accumulation defined by seismic data. Similarly, although the rate of seismic moment release increased dramatically, earthquake locations remained similar to earlier periods. The rate of deformation increased exponentially between April–May 1997 and late November 1997 with a time constant of ~55–65 days, after which it decreased exponentially with about the same time constant. We develop a model consistent with these observations and also consistent with independent constraints on sub-surface rheology from thermal, geochemical and laboratory data. Deformation at sites on the resurgent dome most sensitive to the shallow deformation source are well fit by a model with a single pressure source at 6 km depth which experienced a pressure pulse that began in late 1996, peaked in November 1997, close to the time of major seismic moment release, and essentially ended in mid-1999. The pressure source in our model is surrounded by a 1 km thick "shell" of Maxwell viscoelastic material (shell viscosity 10^{16} Pa s) within an elastic half space, and has peak values that are much lower than corresponding purely elastic half space models. The shell viscosity is characteristic of a weak, deformable solid, e.g. quartz-bearing country rock surrounding the magma chamber at temperatures in the range 500–600°C, i.e. above the brittle–ductile transition, and/or largely crystallized rhyolite near its solidus temperature of ~670°C, material that probably exists near the top of the zoned magma chamber at Long Valley.

Keywords: Long Valley Caldera; viscoelastic rheology; geodetic constraints

1. Introduction

Geodetic data describing surface deformation on active volcanoes can be used to infer the size and shape of magmatic "plumbing systems" at depth, and if available in a timely manner, may also be useful for eruption warning. However, relating strain or displacement at the surface to stress or pressure sources at depth requires assumptions about the rheology of intervening material. This reflects the non-uniqueness of surface deformation data and the inherent tradeoff between source pressure, rheology and other factors. It also suggests the importance of using extra information to help constrain the problem. If the assumed rheology is a

* Corresponding author. Fax: +1-305-361-4632.
E-mail address: tdixon@rsmas.miami.edu (T.H. Dixon).

0377-0273/01/$ - see front matter
PII: S0377-0273(00)00255-9

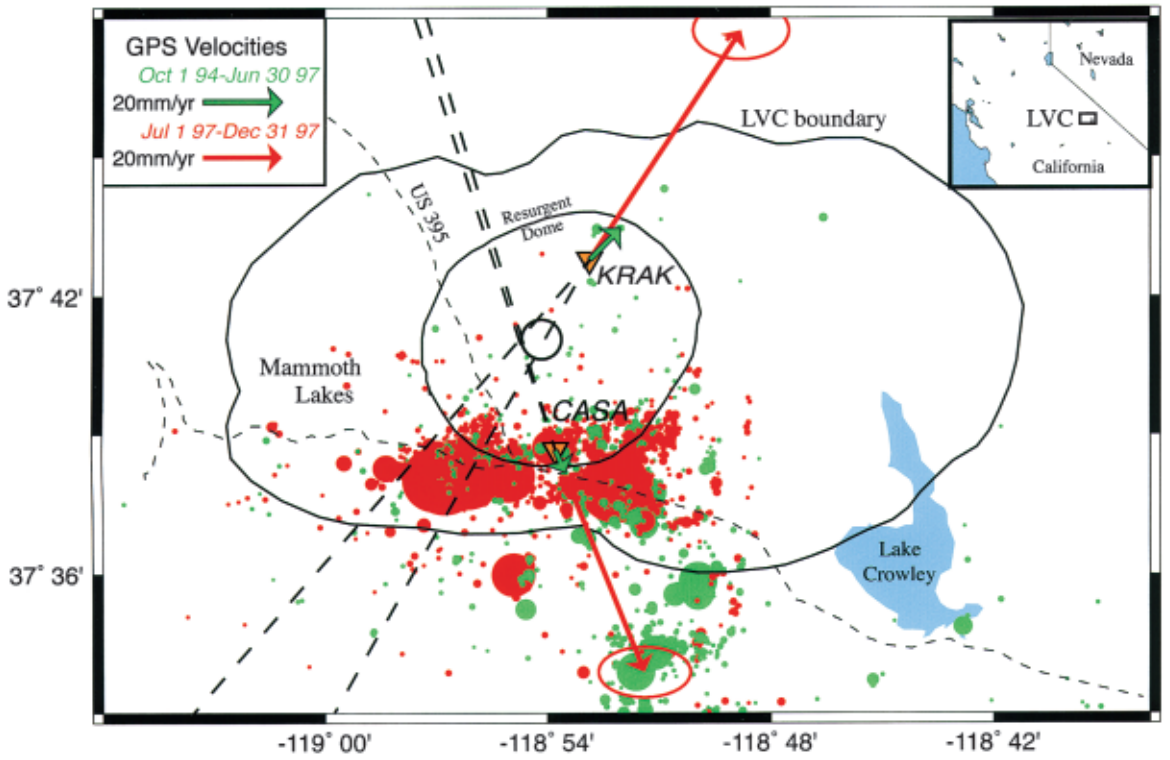

Fig. 1. Sketch map of deformation and seismicity at Long Valley Caldera in eastern California (inset shows location) for two different time periods, color-coded. Geodetic sites CASA and KRAK on central resurgent dome shown as triangles. Deformation rate (arrows with 95% confidence ellipses) and seismicity scaled by magnitude (filled circles) shown for low activity period in green (October 1 1994–June 30 1997) and high activity period in red (July 1 1997–December 31 1998). Dashed lines show the projected intersection point for the GPS data. Open circle between CASA and KRAK shows location and 95% confidence limits of shallow deformation source for the period 1989–1992 described by Langbein et al. (1995). Seismic data were collected and analyzed by the Northern California Earthquake Data Center.

poor representation of reality, deformation data may fit a given model, but inferences about the processes of interest may be wrong.

Most volcano deformation models published to date assume that the earth's crust behaves as a perfectly elastic solid. While elastic half space models fit a variety of crustal deformation data, this rheology is an oversimplification, and may be an especially poor choice for volcanoes, depending on data type, volcano type, and eruption history. The elastic approximation is generally appropriate for small deformations of crustal materials with temperatures cooler than the brittle–ductile transition, about 300–500°C depending mainly on composition and strain rate. Thus, elastic behavior characterizes the upper 10–15 km of the earth's crust in most non-volcanic regions. However, in active volcanic zones, magma at relatively shallow crustal levels can perturb the geothermal gradient significantly. Plastic, viscous, or viscoelastic behavior is more likely to characterize the upper crust near a magmatic center, and can greatly influence the surface deformation field, rendering the elastic approximation inappropriate. Bonafede et al. (1986) and Dragoni and Magnanensi (1989) describe volcano deformation models involving viscoelastic behavior. In this paper we apply the results of these pioneering theoretical studies to data from a recent deformation episode at Long Valley caldera in east-central California.

Long Valley Caldera has experienced seismicity and surface deformation well above background levels since 1979. The most active period in the last century was the initial (1979–1980) inflation episode, with moderately high activity in 1980–1983,

1989–1990 (Hill et al., 1991; Langbein et al., 1993, 1995) and the most recent phase of unrest in mid- and late 1997. This activity almost certainly reflects intrusion of basaltic magma from the upper mantle and/or lower crust into the middle and upper crust (Dvorak and Dzurisin, 1997; Battaglia et al., 1999). Here we examine this recent phase of unrest, interpret it in the context of a model that incorporates viscoelastic rheology near the magma chamber, and show that the predictions of such a model in terms of rheological conditions near the magma chamber are broadly consistent with independent constraints based on thermal and geochemical data from Long Valley and laboratory data on the material properties of quartz-bearing upper crustal rocks.

2. Deformation and seismic data

The deformation data come from two continuously recording GPS stations (CASA, KRAK) separated by about 8 km and spanning the resurgent dome (Dixon et al., 1997), and two-color EDM data from the same locations (Langbein et al., 1995) (Fig. 1). The GPS data were analyzed at the University of Miami's Geodesy Laboratory following Dixon et al. (1997). Briefly, we used the GIPSY software and precise satellite ephemerides provided by the Jet Propulsion Laboratory (Zumberge et al., 1997), analyzing our data in the ITRF-96 reference frame (Sillard et al., 1998). The EDM system is described by Langbein (1989). Previous geodetic studies (Langbein et al., 1993, 1995) have addressed spatial variation in the deformation field based on a variety of geodetic data, placing tight constraints on the location and shape of several deformation sources, including a shallow (5–7 km depth) source of deformation northwest of CASA and southwest of KRAK. Below we argue that the location of this shallow source did not change appreciably during the recent phase of deformation, although the rate of deformation increased markedly over a roughly six-month period. Here we focus on the time-varying aspects of recent deformation associated with the shallow source, well represented by the vector data from the two continuous GPS stations, and the more precise but scalar two-color EDM data from the same locations. More extensive two-color EDM data from other locations show a similar pattern of time variation at sites closest to the resurgent dome (Langbein, personal communication and http://www.usgs.gov/QUAKES/geodetic/twocolor/longvalley.html), but the amplitude of the time-varying signal is largest at CASA and KRAK, making data from these sites ideal for this study.

Seismic event locations and magnitudes were retrieved from the Northern California Earthquake Data Center (http://quake.geo.berkely.edu). The earthquake magnitudes are reported as a combination of coda, local and maximum amplitude magnitudes (M_{coda}, M_l and M_{Mamp}). We converted them to seismic moment, M_0, using an empirical formula for conversion from surface wave magnitude M_s (Hanks and Kanamori, 1979):

$$\log_{10} M_0 = 1.5M_s + 16.1 \quad (1)$$

modified for SI units (N m). Earthquakes in the region represent both volcanic and tectonic sources (e.g. Stroujkova and Malin, 2000), thus determination of seismic moment is not straightforward. The conversion given above was developed for non-volcanic regions, and could yield biased moment estimates for Long Valley. However, for the small magnitude earthquakes under consideration, the differences are not significant, and also have essentially no effect on our estimate of the rate of cumulative moment growth with time, our main concern here.

A map view of seismic data and the horizontal components of the GPS site velocities at CASA and KRAK relative to the stable Sierra Nevada block (Fig. 1) and a vertical section through these sites (Fig. 2) are shown for two periods: October 1994 (beginning of deformation measurements at KRAK) to June 30, 1997 (roughly the beginning of enhanced activity) and July 1, 1997 to December 31, 1997 (roughly the period of high activity). The rate of deformation for the latter period is about one order of magnitude higher than the former (see also the average slopes for the different time periods on the position versus time plot for station CASA in Fig. 3). For the one-year period from July 1, 1997 to June 30, 1998, the elevation of CASA increased by about 7 cm, compared with about 1 cm for the previous 12-month period. Prior to that, elevation increased by about 2 cm/yr from 1994 to 1996. CASA lies about 5 km southeast of the center of maximum uplift for the

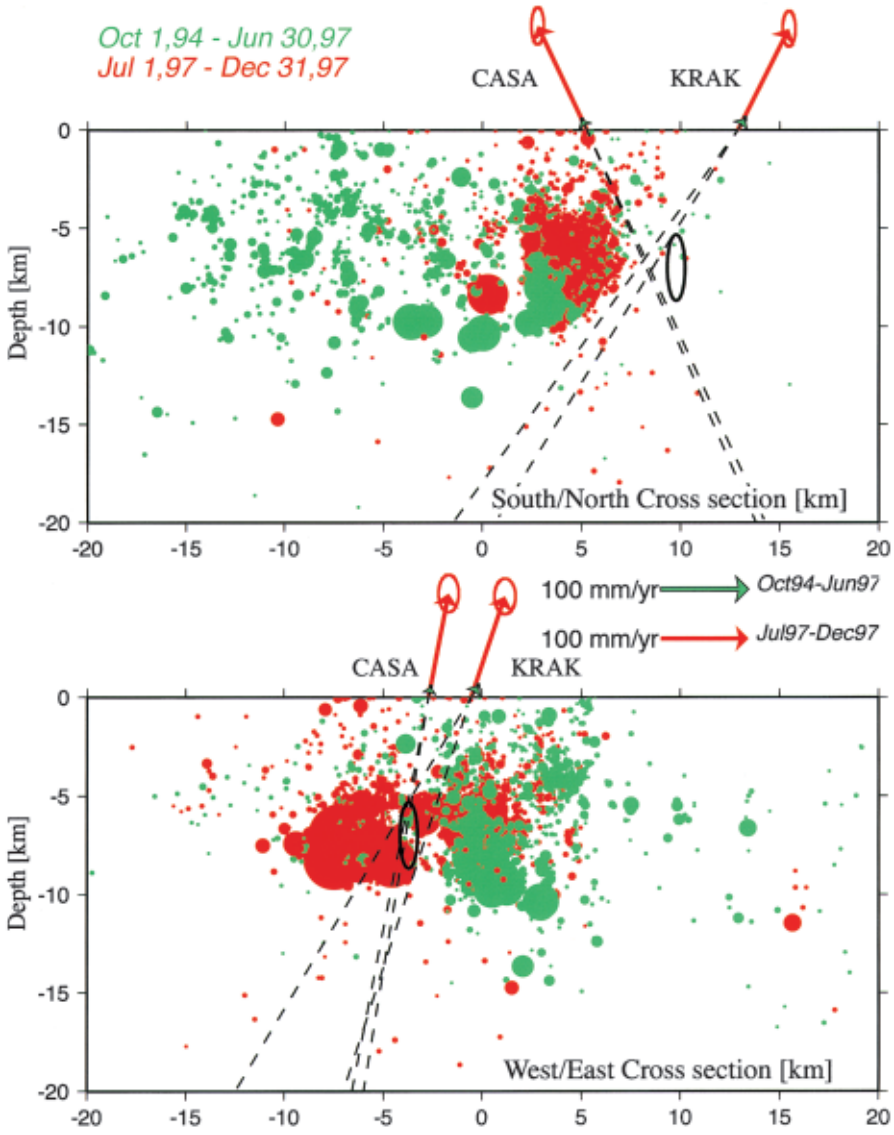

Fig. 2. Similar to Fig. 1, except south–north and west–east cross-sections are displayed, to illustrate depth range of seismicity and vertical component of surface deformation. Note small green arrows at base of the red arrows representing GPS velocity for earlier time periods.

resurgent dome (Langbein et al., 1995; Dvorak and Dzurisin, 1997). Uplift rates at this center location are about a factor of two higher compared to CASA. Adding this latest phase of uplift to previously measured uplift from leveling at this location (Dvorak and Dzurisin, 1997) indicates that from inception of uplift sometime after 1975 (probably 1979) to late 1998, this central location increased in elevation by about 75 cm. Roughly 15% of this uplift occurred between mid-1997 and early 1998.

Langbein et al. (1995) used geodetic data to 1992 to suggest the presence of a shallow source of deformation (5–7 km) beneath the resurgent dome, plus a deeper source at about 13 km, and a dike beneath Mammoth Mountain. The motions of CASA and KRAK mainly reflect pressure or volume changes in

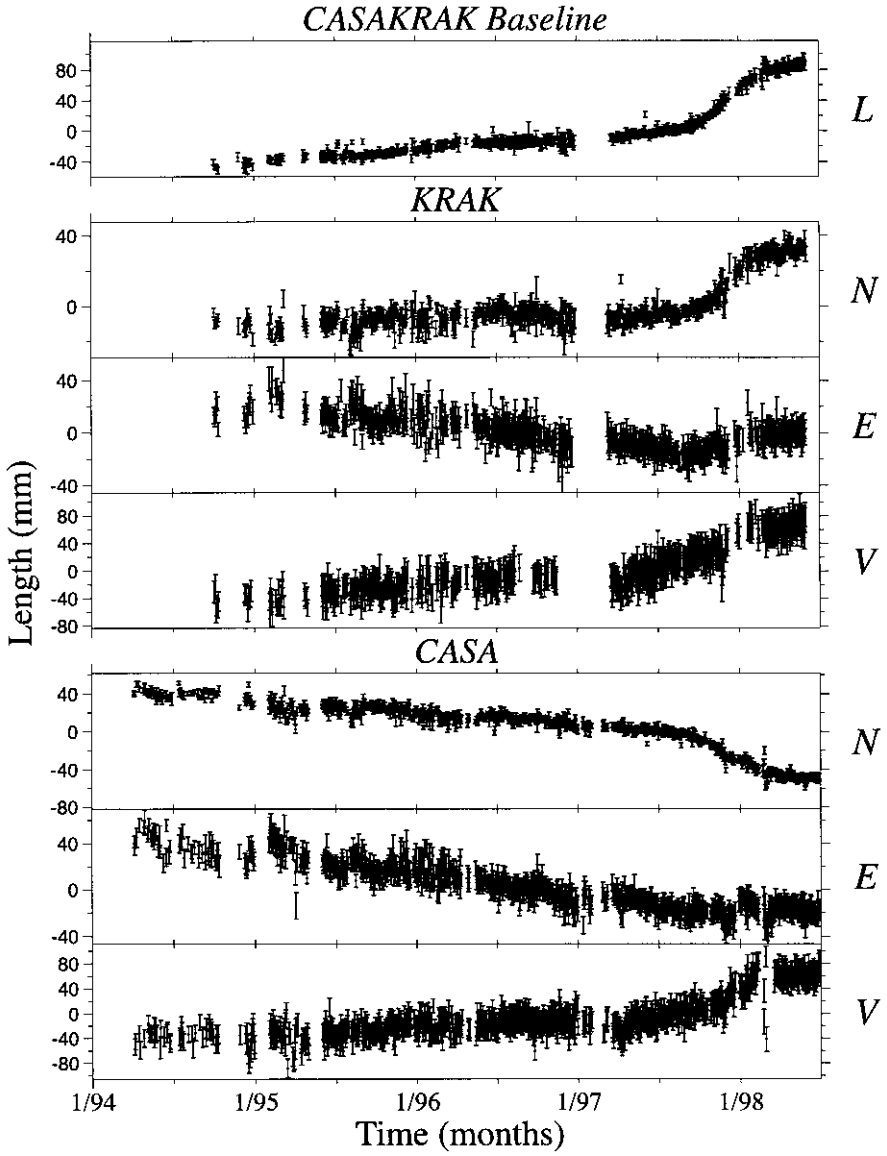

Fig. 3. Time series of daily vector position components estimated by GPS at stations CASA and KRAK and scalar length between CASA and KRAK for 1994–1998 relative to arbitrary initial positions. Data points with large formal errors (north ≥8.0 mm, east ≥12.0 mm, vertical ≥20.0 mm, length ≥10.0 mm) were removed.

the shallow source beneath the resurgent dome. It is these data which we hope to use as a probe of processes in the shallow crust beneath the resurgent dome. The orientation of vectors in Fig. 1 suggests that the horizontal position of the shallow source responsible for surface deformation at CASA and KRAK (intersection of vectors) has not changed appreciably during the most recent phase of activity compared to the previous several years.

An important question for volcanic hazard assessment is whether the increased rate of surface deformation and seismicity reflects movement of magma significantly closer to the surface. The vertical component of deformation, when combined with the

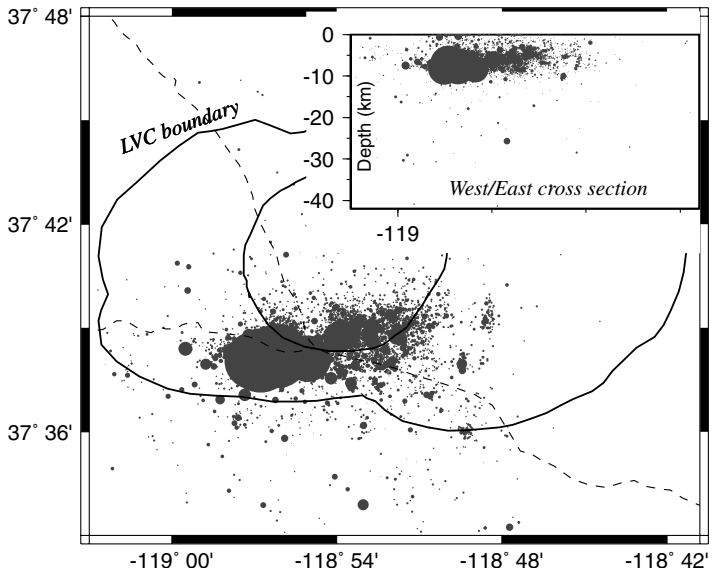

Fig. 4. Seismicity at Long Valley for November 1997. Inset shows all events in map view projected onto a west-east cross section. Note well-defined linear trend, which may indicate location of a dike or fault near the south moat.

horizontal components can be used to address this question. Fig. 2 includes the vertical component of deformation for the same periods as Fig. 1. There is no suggestion in these data that the deformation source depth has changed significantly, as evidenced by the similar orientation of surface displacement vectors for the two periods. Following Dixon et al. (1997) we can estimate the depth of deformation assuming a simple point source (Mogi, 1958). For January 1, 1994 to June 30, 1997 we obtain 6.1 ± 0.7 km (one standard error), and for July 1, 1997 to December 31, 1998 we obtain 7.7 ± 0.5 km. Dixon et al. (1997) reported a depth of 5.8 ± 1.6 km for the period January 1, 1995 to December 31, 1995. Langbein et al. (1995) reported a depth range of 5.5–7.0 km for this shallow source, using deformation data for the period 1988–1992, and incorporating an ellipsoidal point source model. All of these depths are equivalent at 95% confidence. While we suspect that magma has indeed moved upward during this period, the majority of this motion may be in the deeper parts of the magma chamber, and may have little effect of the surface deformation at CASA and KRAK. These stations appear to respond to pressure changes at shallower levels, perhaps near the top of the magma chamber, as discussed in a subsequent section.

Similarly, the location of seismicity has not migrated significantly during this period, either horizontally (Fig. 1) or vertically (Fig. 2). In contrast to the source of shallow deformation beneath the resurgent dome, seismicity is concentrated along the southern rim of the caldera, the south moat, an area of enhanced seismic activity since 1979. Prior to the recent phase of activity, earthquakes were relatively disperse, including many events southeast of the moat along the Hilton Creek fault (Fig. 1). During the swarm activity that began in July 1997 and continuing through January 1998, earthquakes became more focussed, defining a near-vertical, east-west-striking plane or tabular body about 15 km long, extending to a depth of about 10 km (Fig. 4). Savage and Cockerham (1984) and Savage et al. (1987) postulated the existence of an active dike near here as well as right lateral slip during the 1982–1983 inflation episode, a period that included a seismic swarm similar in some respects to the 1997 activity. Thus the enhanced rate of seismicity in mid- and late 1997 might reflect a dike that expanded more rapidly or a fault that slipped more frequently in this period compared to the previous few years (Langbein et al., 1998). It does not appear to be directly related to pressure or volume increases immediately beneath the resurgent dome,

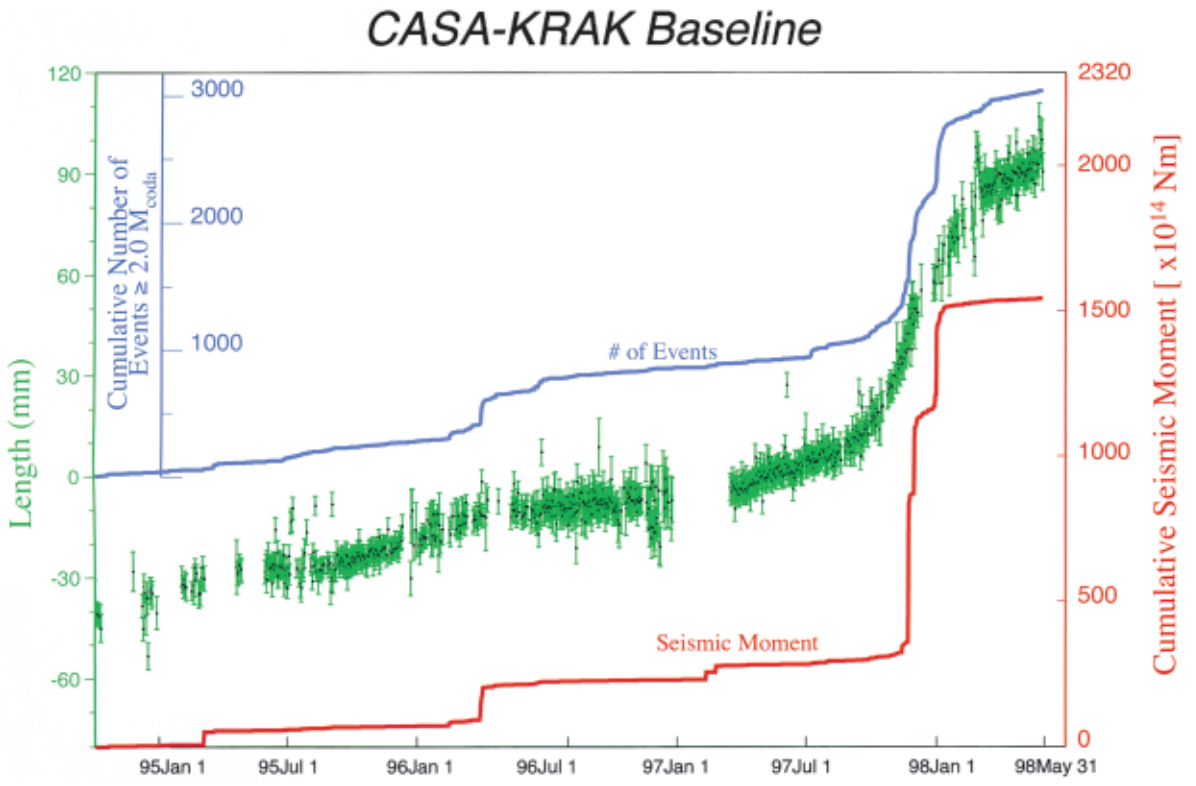

Fig. 5. Scalar length between CASA and KRAK measured by GPS minus an arbitrary constant, compared to cumulative seismic moment and cumulative number of seismic events with $M_{coda} \geq 2.0$ for the period October 1994–June 1998.

since it is in a different location, although we will later describe a model that links these processes.

The relative timing of increased seismicity and deformation is important for understanding the nature of stress buildup in the crust. Langbein et al. (1993) noted that increased deformation in late 1989 preceded increased seismic moment release (energy release) by several months. Fig. 5 shows GPS observations at CASA and KRAK from late 1994 to mid-1998, along with cumulative seismic moment and cumulative number of events with coda-duration magnitudes ≥2.0. Increased deformation rate is noticeable beginning about July or August 1997, but the greatest release of seismic moment occurs several months later, in November 1997, similar to the 1989–1990 pattern. On the other hand, cumulative number of earthquakes increases at about the same time as increased deformation rate, so the time lag in seismic energy release reflects the timing of a few large events, not the onset of increased rate of seismicity. A small increase in deformation rate in late 1995–early 1996 may have followed a similar pattern, since seismicity increased somewhat later, in March–April 1996 (Fig. 5). In the model to be presented, we will show that the major seismic moment release in late 1997 occurs at the time of maximum pressure near the top of the magma chamber.

2.1. Exponential changes in deformation rate

A fascinating feature of the recent activity at Long Valley is the exponential increase in surface deformation rate beginning around June or July 1997 and ending in December 1997, followed by an exponential decay. Fig. 5 shows the GPS-determined length between CASA and KRAK for the period October 1, 1994 to June 30, 1998. The large exponential increase (June–December 1997) in these data can be fit by a linear growth with superimposed exponential

Table 1
Characteristic time ($\tau_{1,2}$) and goodness-of-fit (χ^2 per degree of freedom, reduced χ^2) for CASA and KRAK GPS position vector components, and scalar baseline length between KRAK and CASA for GPS and two color EDM. Fits for the GPS east components are not possible due to low signal to noise ratio

Baseline component		Growth		Decay	
		τ_1 (days)	Reduced χ^2	τ_2 (days)	Reduced χ^2
GPS					
CASA	N	63	2.1	79	2.2
CASA	V	70	0.6	83	0.9
KRAK	N	79	1.3	34	0.6
KRAK	V	67	0.6	39	0.4
CASA–KRAK	L	56	0.8	66	1.0
EDM					
CASA–KRAK	L	64	3.0	61	4.4

increase:

$$u(t) = rt + e^{[(t-t_1)/\tau_1]} \quad (2)$$

where $u(t)$ is the position component as a function of time, r is the rate of linear displacement, t_1 is the start time of the exponential process, and τ_1 is the exponential time constant (characteristic time) during this phase. In this example, the best fitting value for τ_1 for the GPS baseline between CASA and KRAK is 56

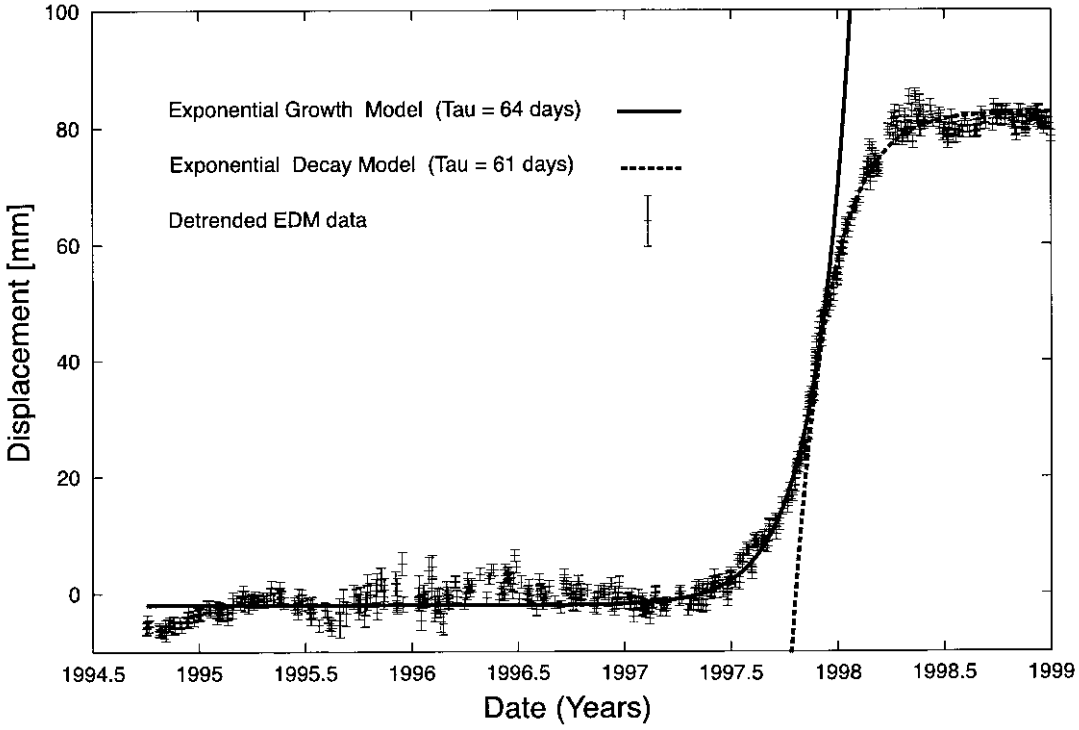

Fig. 6. Scalar length between CASA and KRAK measured by two-color EDM, detrended by 15 mm/yr, with exponential fits for early (increasing deformation rate) and later (decreasing deformation rate) periods.

days. Similarly, the later part of the time series can be fit by exponential decay superimposed with the same linear growth from Eq. (2):

$$u(t) = rt - e^{[-(t-t_2)/\tau_2]} \quad (3)$$

with t_2 now the stop time of the exponential process, and $\tau_2 = 66$ days. We also fit this model to coordinate velocities (individual motions of CASA and KRAK; e.g. Fig. 3). Roughly similar characteristic times are obtained regardless of velocity component (Table 1), although the signal to noise ratio in the east component is too low to extract a reliable estimate. While the standard error is greatest in the vertical component (e.g. Mao et al., 1999), the signal is also larger (Fig. 3), enabling an estimate. Depending on component and station, we obtain values of τ between 34 and 83 days for the various GPS data (Table 1). The most precise estimate of τ comes from the two-color EDM data for the CASA–KRAK baseline, giving $\tau_1 = 64$ days, and $\tau_2 = 61$ days (Fig. 6). We have not done a formal error analysis for our estimates of characteristic time, but numerical simulations suggest that the better determined (e.g. EDM length) components have uncertainties ($\pm$one standard error) of about ± 5 days, while more poorly determined components (e.g. GPS vertical) have uncertainties of about ± 20 days. Thus, all the estimates quoted above are equivalent within error, and the characteristic times are similar for both the growth and decay phases of the deformation episode. In the subsequent discussion we take a value of 60 days as representative for both periods, and consider a range of 34–83 days.

We suggest that the characteristic time is a useful parameter for describing the deformation episode, since the data are well fit by a simple exponential function and the values are similar for both the exponentially increasing and decreasing parts of the episode. Basaltic systems on Iceland and Hawaii also sometimes exhibit deformation episodes with exponentially increasing or decreasing deformation rates (e.g. Trygvason, 1980; Dvorak and Okamura, 1987; Linde et al., 1994; Owen et al., 1997; Dvorak and Dzurisin, 1997) but typically the characteristic deformation times are less than 1.5 days, sometimes just a few hours, considerably shorter than the Long Valley example. Many of the Hawaii and Iceland data referenced above indicate relaxation times associated with abrupt withdrawal of basaltic magma from a reservoir and subsequent relaxation of the system. Also, in some cases these data consist of strain or tilt as opposed to displacement measurements; for the order of magnitude comparisons of interest here, this difference is not important, although note that strain/tilt measurement systems tend not to record long-lived deformation events due to instrument drift. In comparing these various phenomena we assume that there is useful information in the characteristic time for exponentially changing surface deformation time series, independent of the sign of the exponent or whether the time series is exponentially decreasing or increasing. Whether this is a function of the underlying process (magma intrusion), a response of the crustal media into which the magma intrudes, or both, remains to be determined, and likely differs at different volcanoes and at different times for a given volcano. Nevertheless, based on the limited data available, it appears that deformation at basaltic volcanoes can often be characterized by relatively short time constants, typically one day or less, compared to much longer times that may be observed at Long Valley, a more silicic system. It is likely that temperature, magma viscosity and the composition of the country rock all affect characteristic deformation time, with hot, basaltic systems characterized by rapid migration of low viscosity magma through dikes or conduits and short deformation times, while cooler, higher viscosity rhyolitic systems or zoned basaltic–rhyolitic systems sometimes exhibit longer characteristic times.

3. A model for surface deformation

A large number of models could explain the observed exponential surface deformation at Long Valley, reflecting the inherent non-uniqueness of surface deformation data. For example, a period of enhanced surface deformation could reflect: (a) a change in the position of the pressure source (closer to the surface) with constant source strength and rheology; (b) a change in the rheology of intervening material (decrease in material strength) with constant source strength and source position; (c) a change in source strength, with source position and surrounding rheology remaining constant; or some combination.

Each of the above models may also assume simple elastic half space rheology (for example, scenario (b) could be implemented by simply changing the elastic shear modulus as a function of time), or a more realistic, but more complex, rheological structure.

From surface geodetic data alone, it is not possible to distinguish among these models. However, much additional evidence is available to help constrain the problem. Recall that the three dimensional vector GPS data suggest that source location did not change significantly during the deformation episode, either in the horizontal (Fig. 1) or vertical (Fig. 2) sense, allowing us to rule out scenario (a). Strain rate-dependent rheology (strain weakening) could lead to scenario (b). In this paper we focus on scenario (c) as it is plausible and straightforward to test. We next consider independent evidence for the rheological structure of the volcano.

Thermal considerations suggest that for any long-lived magmatic system, rocks near the magma chamber will be elevated above the brittle–ductile transition temperature, and thus may not behave elastically, depending on the time scale of deformation. Laboratory data to be discussed suggest that many crustal materials heated above the brittle-ductile transition temperature, as well as cooling rhyolitic liquids, can be modeled as viscoelastic substances. Finally, models incorporating viscoelastic rheology often predict deformation that varies exponentially in time, as observed at Long Valley in the 1997–1998 deformation episode.

In the model to be described, we assume that the viscoelastic properties of rhyolitic material near the top of the magma chamber, and/or hot country rock nearby, play an important role in controlling the surface deformation field near the resurgent dome.

3.1. Zoned magma chambers

Before attempting to formulate and test a specific model, we review current ideas about the nature of the magmatic system at Long Valley and other silicic calderas. A variety of field, petrological and geochemical observations suggest that magma chambers in these systems are zoned or stratified, with lower density, higher viscosity rhyolitic melts overlying higher density, lower viscosity basaltic melts, or their solidified equivalents (e.g. Eichelburger and Gooley, 1977; Hildreth, 1981; Dvorak and Dzurisin, 1997). This gradation reflects the process by which rhyolitic magmas are thought to be generated, whereby basaltic magma from the upper mantle or lower crust intrudes into the middle or upper crust (the likely level of neutral buoyancy), interacts with more silica-rich country rock, and forms rhyolite mainly by combined differentiation and assimilation (Christiansen and Lipman, 1972; Hildreth, 1981; Dvorak and Dzurisin, 1997). Most magma that is eventually extruded at Long Valley has a silicic composition, including the Holocene rhyolitic lavas and pyroclastic material erupted along the Inyo volcanic chain at the northwest end of the caldera (Miller, 1985; Fink, 1985; Vogel et al., 1989). However, petrologic evidence suggests that silicic eruptions are often "triggered" by a pulse of basaltic magma intruded into the lower magma chamber (Sparks et al., 1977; Johnston, 1978; Bailey, 1984; Pallister et al., 1992). At Long Valley, basalt injection and mixing may have triggered post-caldera silicic volcanism at 0.3 Ma (Bailey, 1984) and the 600-year-old Inyo eruption (Varga et al., 1990).

Basaltic eruptions have been relatively common at Long Valley in the last 400,000 years (Mankinen et al., 1986; Bailey, 1989; Vogel et al., 1994; Cousens, 1996), and their mode of eruption may also reflect magma chamber stratification and the contrasting properties of basaltic and rhyolitic magma. Young basaltic eruptions tend to be concentrated around the margins of the resurgent dome, implying that their rise within the magma chamber is hindered by the lower density, higher viscosity rhyolitic "cap" at the top, forcing rising basaltic magma to migrate laterally and "leak out" around the edges (e.g. Bailey, 1984, 1989).

Most seismic studies agree that a likely explanation for the unrest at Long Valley beginning in 1979 is related to intrusion of new magma, based on low P-wave velocities, high attenuation of S waves, and other seismic anomalies indicative of the presence of magma or fluid (e.g. Rundle et al., 1985; Rundle and Hill, 1988; Hill et al., 1990). High attenuation of seismic energy in the depth range 6–12 km beneath the resurgent dome (Steck and Prothero, 1994; Sanders et al., 1995; Sanders and Nixon, 1995), may define the magma chamber, or at least region where

magma or fluid is present in amounts sufficient to affect seismic waves. A recent study exploiting the intense earthquake swarm of 1997 places the top of this possible magma chamber at one location near CASA (the swarm location) at a depth of 7.8 km (Stroujkova and Malin, 2000). Due to their location and the general relation of surface deformation to pressure changes at depth, CASA and KRAK are more sensitive to shallow (less than 10 km) processes compared to deeper-seated processes, even though the latter are likely to be more fundamental in controlling long-term evolution of the system. Thus the dominant source of deformation at CASA and KRAK, at a depth of 5–7 km, appears to be located near the top of the seismically defined magma chamber. Since the magma chamber is likely zoned, deformation at CASA and KRAK probably reflects expansion or pressure increase within the uppermost, rhyolitic part of the chamber, or the region immediately above it. This may be in response to heating or advective addition of magma from below, increased volume of volatiles exsolving from rising magma and collecting near the top of the chamber, or thermal expansion of the region immediately above the magma chamber, although the details of the ultimate source of activity (presumably deeper-seated magmatic processes) need not concern us here.

3.2. Thermal zone around a magma chamber

The rheological properties of the solidified (but presumably heated) country rock immediately surrounding the magma chamber may also play an important role in surface deformation, mediating the effect of deeper pressure variations. Thermal considerations suggest that for long-lived volcanic systems, a considerable thickness of country rock around the magma chamber may be heated above the brittle–ductile transition temperature, and thus will not behave in a perfectly elastic manner. Long Valley's eruption history suggests that it has the longevity to generate a relatively wide heated zone, even in the presence of vigorous hydrothermal activity. The system has been active for at least the last 2 Ma (Bailey et al., 1976; Metz and Mahood, 1985). Although the last major eruption, which formed the Bishop Tuff and the present caldera (Bailey et al., 1976; Hildreth and Mahood, 1986), occurred at 760,000 Ma (Izett and Obradovitch, 1994) both basaltic and rhyolitic eruptions have occurred in the last 200,000 years (Mankinen et al., 1986; Bailey, 1989; Varga et al., 1990; Vogel et al., 1994). The most recent rhyolitic eruptions occurred along the southern part of the Mono–Inyo chain about 650 years ago (Miller, 1985; Sieh and Bursik, 1986; Eichelburger et al., 1988). This activity may be sufficient to develop a large, stratified magma chamber as well as a considerable thickness of heated country rock around it, and maintain these features for a considerable length of time.

Field observations of eroded magmatic systems suggest that high temperature contact metamorphic aureoles surrounding these systems have dimensions ranging from a few meters to a few kilometers, with the smaller dimensions characteristic of smaller and/or relatively dry magmatic systems, and the larger dimensions characteristic of larger and/or relatively wet systems, where fluids can advect heat far from the magma chamber boundary. For example, oxygen isotope and mineral stability data for the aureole surrounding the Alta granitic stock in Utah indicate temperatures of 350°C or higher up to 1.5 km from the intrusive boundary (Marchildon and Dipple, 1998). Studies of the Ballachulish aureole in Scotland suggest temperatures in excess of 350°C 2 km or more from that magmatic boundary (Ferry, 1996). We interpret such metamorphic aureoles as representative of thermal boundary zones or "shells" that surround modern magma chambers. Because of the relatively high temperatures in these boundary zones, their mechanical behavior can be modeled as viscoelastic. Evidence discussed below suggests that Long Valley rhyolites are relatively wet, thus the corresponding thermal boundary zone is likely to be relatively wide. In most of the models considered below we set the shell diameter at 1.0 km.

3.3. Viscoelastic shell model

We now describe a model for observed deformation on the resurgent dome. Although non-unique, the model is consistent with all available data, including our current understanding about the structure and composition of zoned magma chambers and thermal and rheological considerations about the country rock immediately surrounding the magma chamber.

Consider a silicic magma chamber experiencing a new influx of basaltic magma from below. If the overlying material has an elastic rheology (e.g. low temperature silicate rock), the pressure increase associated with this influx is immediately expressed by deformation at the surface. However, if the overlying material has a viscoelastic rheology, there is a time dependence to the surface response that depends on the viscosity of the material. High temperature rhyolite at the top of the magma chamber, or country rock surrounding the magma chamber that is heated above the brittle–ductile transition, can be considered a viscoelastic boundary zone or shell around the magma chamber.

For a relatively wide range of temperatures and strain rates, rhyolites and granites above the brittle–ductile transition temperature can be characterized as Maxwell viscoelastic solids (Dingwell and Webb, 1989; Dingwell, 1995; Richet and Bottinga, 1995; Webb and Dingwell, 1995). The behavior of Maxwell solids can be illustrated with a simple mechanical analogue, a spring and dashpot (piston–cylinder arrangement) in series, representing the elastic and viscous parts of the response, respectively. Maxwell solids are often characterized by two parameters, the rigidity, G (also known as the shear modulus), which describes short-term elastic (unrelaxed) behavior, and the Newtonian shear viscosity, η, which describes longer-term viscous (relaxed) behavior. For such materials, the relation between characteristic response time (Maxwell time), τ, shear viscosity, and rigidity is:

$$\tau = \eta/G \tag{4}$$

These quantities differ depending on whether the applied stress is shear or volumetric, but the difference is small and can be ignored here (Dingwell and Webb, 1989; Dingwell, 1995). For time scales much shorter than the characteristic time, elastic behavior (the "spring") dominates, while for longer times, viscous behavior (the "dashpot") dominates. Since G is similar for most silicate glasses ($\log_{10} G = 100.5$; Dingwell and Webb, 1989), and indeed for most crustal materials, the shear viscosity of the material can be estimated from the characteristic time. Eq. (4) is sometimes written as $\tau = 2\eta/G$. Again the difference is small compared to the order of magnitude estimates for viscosity of interest here.

Dragoni and Magnanensi (1989) describe a viscoelastic shell model for volcano deformation, with a spherical pressure source (e.g. magma chamber) surrounded by a concentric, spherical, Maxwell viscoelastic shell, both embedded in an elastic full space (infinite domain). While a viscosity gradient almost certainly exists near the magma chamber, with lower viscosity material immediately adjacent to the pressure source grading to higher viscosity material further away, a single shell with an average viscosity is probably an adequate approximation. Even with this assumption, up to six parameters describing the material properties are required to completely specify the rheology of the system. For the elastic material these are the bulk modulus, K_1, and shear modulus, G_1. For the viscoelastic material these are the bulk modulus, K_2, and volume viscosity, describing the material response to volumetric stresses, and shear modulus, G_2, and shear viscosity, η, describing the material response to shear stresses. Following Dragoni and Magnanensi (1989), we assume that the shell responds viscously to shear stresses but elastically to volume stresses, i.e. effects related to volume viscosity (sometimes termed pressure viscosity) are ignored. Second, the shear moduli of the two materials are assumed to be equal ($G_1 = G_2 = G$). Third, we assume $K = 5/3G$. This is equivalent to assuming that Poisson's ratio, ν, throughout both materials is constant and equal to 0.25. Finally, we assume that there is little variation in G throughout the crust, consequently this parameter can be fixed to a single value. We set it to 5×10^9 Pa (e.g. Bonafede et al., 1986), somewhat lower than standard crustal values ($1–3 \times 10^{10}$ Pa) and perhaps representative of volcanic regions. Thus instead of six material properties, we need only specify three (G, ν, and η), of which only one (η) is varied in our models. Additional work is needed to assess the validity of these assumptions, define plausible values for the rheological parameters, and determine the extent to which these parameters vary in the region of high thermal gradients near the magma chamber.

For a step-like, instantaneous pressure change, the radial displacement, $u_r(r, t)$ for the viscoelastic shell

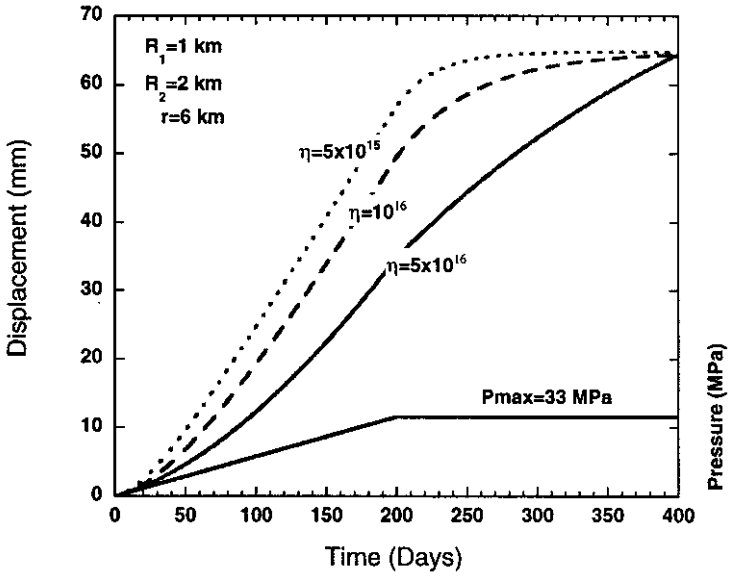

Fig. 7. Deformation predicted by the analytical model of Dragoni and Magnanensi (1989) for the simple pressure history shown, 6 km from a pressure source surrounded by a 1-km-thick viscoelastic shell.

model is:

$$u_r(r,t) = \frac{1}{4}\frac{P_0}{G}\frac{R_2^3}{r^3}\left[1 - \left(1 - \frac{R_1^3}{R_2^3}\right)e^{-t/\tau}\right] \quad (5a)$$

(valid for $r \geq R_2$), where P_0 is the pressure increment, t is time, R_1 is the radius of the pressurized cavity (magma chamber?), R_2 is the radius of the larger viscoelastic shell, and τ is the characteristic time whose definition is modified to account for the physical dimensions of the shell:

$$\tau = \frac{9}{5}\frac{\eta}{G}\left(\frac{R_2}{R_1}\right)^3 \quad (5b)$$

Note that Eq. (5a) predicts displacement that is an exponential function of time, even though the pressure change is instantaneous, i.e. the viscoelastic response of the shell "filters" the effect of the pressure change.

For a more realistic trapezoidal pressure history, where pressure grows linearly with time from 0 to t_1, remains constant until t_2, then decays to 0 by t_3, the radial displacement for the viscoelastic shell model of Dragoni and Magnanensi (1989) is:

$$u_r(r,t) = \frac{1}{4}\frac{P_0}{G}\frac{R_2^3}{r^2}\left[f_1(t) - \left(1 - \frac{R_1^3}{R_2^3}\right)f_2(t)\right] \quad (6a)$$

where

$$f_1(t) = \frac{t - (t-t_1)H(t-t_1)}{t_1} + \frac{(t-t_3)H(t-t_3) - (t-t_2)H(t-t_2)}{t_3 - t_2} \quad (6b)$$

$$f_2(t) = \tau\left(\frac{M-N}{t_1} + \frac{O-P}{t_3-t_2}\right) \quad (6c)$$

$$M = 1 - e^{-t/\tau} \quad (6d)$$

$$N = H(t-t_1)\{1 - e^{-(t-t_1)/\tau}\} \quad (6e)$$

$$O = H(t-t_3)\{1 - e^{-(t-t_3)/\tau}\} \quad (6f)$$

$$P = H(t-t_2)\{1 - e^{-(t-t_2)/\tau}\} \quad (6g)$$

$H(t)$ is the Heaviside step function ($H = 1$ when $t > 0$ and $H = 0$ for $t < 0$), and τ is defined by Eq. (5b). Again, the model predicts deformation outside the shell that has an exponential dependence on time.

By analogy with the Mogi elastic model (Mogi, 1958) the viscoelastic shell model is a point-like source model, in the sense that the size of the source (R_1) cannot be uniquely determined from geodetic

data alone given the trade-off between source dimension and source pressure (P).

Fig. 7 shows the deformation predicted by such a model for several values of shell viscosity and a simple pressure history, namely a linear increase to some maximum pressure, which then remains constant. Note that although the pressure history in this example is piecewise linear, the predicted surface deformation is non-linear, depends on shell viscosity, and is crudely similar to the pattern observed at Long Valley. While this simple, two stage pressure model cannot exactly match the pattern of surface deformation, it does suggest that at least some of the "curvature" in the deformation pattern might be related to the properties of viscoelastic material at depth.

In order to quantitatively compare predictions of the viscoelastic shell model to the deformation data, we require constraints on the dimensions and viscosity of the shell, the ability to specify more sophisticated pressure histories, and knowledge of the effect of the free surface on the model predictions (the available analytical solution is valid only for an elastic full space; we require a half space model).

3.3.1. Shell dimensions and viscosity

At first glance it might appear that estimates for the shell viscosity are highly non-unique, being functions of τ, R_1 and R_2 (Eq. (5b)). However, while the absolute dimensions of magma chambers and their high temperature aureoles must vary greatly, variation in the ratio R_2/R_1 is probably much less, since small magma chambers tend to heat relatively small volumes of adjacent country rock, while large magma chambers heat correspondingly larger volumes. For $R_2/R_1 = 1.5$–3.0 (a typical range?), and $\tau \sim 60$ days, the variation in viscosity predicted by the model is only about one order of magnitude (Fig. 8). In contrast, for plausible temperature and compositional ranges of volcanic materials, viscosity can vary by at least 10 orders of magnitude. This suggests that characteristic times for surface deformation in the viscoelastic shell model largely depend on the rheological characteristics of the region near the pressure source. Perhaps surface deformation data might be used to "probe" this otherwise inaccessible region. For $\tau = 34$–83 days and the simple model described above, the implied average viscosity of the shell is $\sim 3 \times 10^{14}$–10^{16} Pa s, the viscosity of an easily deformable solid.

This viscosity range is broadly consistent with our expectations. For example, it is several orders of magnitude lower than typical lower crustal viscosities in non-volcanic regions, generally considered to be in the range 10^{19}–10^{20} Pa s (e.g. Thatcher, 1983; Savage

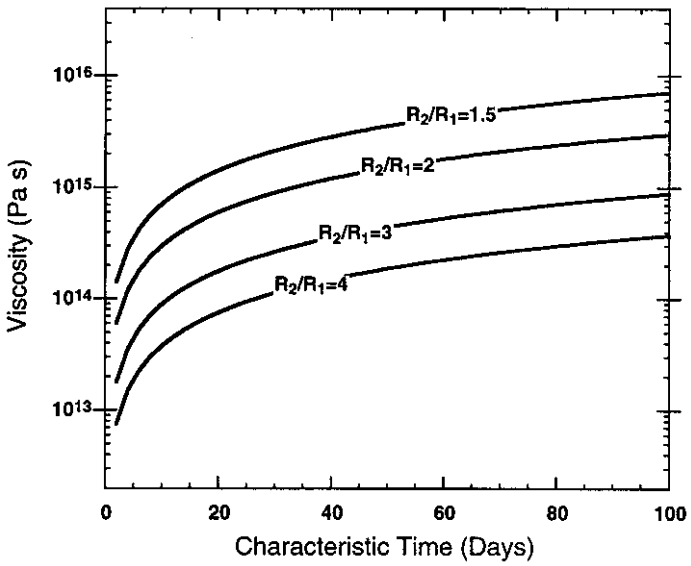

Fig. 8. Characteristic time, τ, versus shear viscosity, η, for various R_2/R_1 (Eq. (5b), text).

and Lisowski, 1998; Dixon et al., 2000; Kenner and Segall, 2000; Pollitz et al., 2000). Typical lower crust is probably more mafic in composition than upper crustal material at Long Valley and may also be cooler, implying higher viscosity.

Consideration of the petrological and thermal conditions of the magma chamber and surrounding country rock provides additional information on viscosity. At a depth of 6 km, near the top of the seismically defined magma chamber at Long Valley and equivalent to the shallow deformation source whose effects dominate CASA and KRAK site velocities, temperatures probably lie in the range 450–800°C, depending in part on assumptions about the extent of shallow hydrothermal circulation and the actual location of the magma chamber (Sorey, 1985; Hill, 1992). The solidus temperature for wet rhyolite lies in the middle of this range, 670°C (e.g. Winkler, 1974; Maaløe and Wyllie, 1975). If rhyolite is present in significant quantities at the top of the magma chamber, it will act as a thermal "buffer," maintaining the temperature of the surroundings near this value for a considerable length of time. We will consider first the viscosity of the rhyolitic cap at the top of the magma chamber as a function of water content, temperature and crystal content. Second, we will consider the temperature dependence of the viscosity of the surrounding country rock.

The viscosity of a rhyolitic melt is a strong function of water content. Studies of melt inclusions in quartz in the Bishop Tuff indicate that rhyolites produced at Long Valley during this eruption had pre-eruptive water contents of 2–7 wt% (Newman et al., 1988; Anderson et al., 1989; Skirius, 1990; Dunbar and Hervig, 1992; Wallace et al., 1995), which reduces the viscosity 6–7 log units relative to dry rhyolite (Neuville et al., 1993; Richet et al., 1996; Schulze et al., 1996). In the following discussion we take a value of 5% water as representative. The viscosity of wet rhyolitic melt is $\sim 10^5$–10^8 Pa s at temperatures of 650–800°C (wet rhyolite curve on Fig. 9), significantly lower than the viscosity we infer from the deformation time constant and the viscoelastic shell model ($\sim 10^{14}$–10^{16} Pa s).

The existence of completely molten rhyolite at the top of the magma chamber, however, is unlikely. For the more likely case of a partly to largely crystallized rhyolite, studies of the rheology of crystal-bearing silicate melts (e.g. Marsh, 1981; Lejeune and Richet, 1995) and partially-melted granites (e.g. Arzi, 1978a,b; van der Molen and Paterson, 1979) show that viscosity varies nonlinearly with crystal content, and is best described over three distinct intervals of crystallinity. Between 0 and ~40% crystals, the system behaves as a suspension of well-separated crystals in a melt, and can be considered a simple Newtonian fluid. Addition of up to ~40% crystals will result in a viscosity increase of <1 log unit. Between ~40 and ~70% crystals, the system transitions from being suspension-controlled to being granular-controlled. Viscosity increases sharply by ~6 log units over this crystallization interval. At crystal contents >70%, the viscosity continues to increase with crystal content, but gradually reaches a maximum of ~8–10 log units greater than that of the homogeneous liquid. Addition of 80–90 vol% crystals to a homogeneous liquid increases the viscosity ~7.5–9 log units above the crystal-free melt (Fig. 9). At these high crystal contents, non-Newtonian behavior becomes important, although an effective Newtonian viscosity can still be defined. A hypothetical crystallization–temperature–viscosity path with crystal content and viscosity increasing sharply near the solidus temperature is also shown in Fig. 9. A mostly crystalline, wet rhyolite would have a viscosity of $\sim 10^{15}$–10^{17} Pa s at or near the solidus temperature of 670°C, similar to the values inferred from our model.

Another candidate material for the viscoelastic shell is the crystalline country rock surrounding the magma chamber, material that is presumably somewhat cooler than the magma chamber, but considerably warmer than crust at equivalent depth outside the active volcanic region. At temperatures above about 300–350°C, the rheological behavior of most upper crustal rocks will likely be dominated by ductile deformation of its weakest component, quartz, as long as quartz makes up at least ~10–15% of the rock. This condition is likely satisfied for the Paleozoic metasediments, Mesozoic metavolcanics, and Cretaceous granodiorites (Sierran batholithic rocks) that comprise the country rock for the Long Valley magma chamber (Bailey, 1989). Above 300–350°C, quartz deforms by power law (non-Newtonian) dislocation creep (Brace and Kohlstedt, 1980; Kirby and Kronenburg, 1987). It is nevertheless possible to define an effective Newtonian viscosity at a given strain rate. Based on experimental determinations of

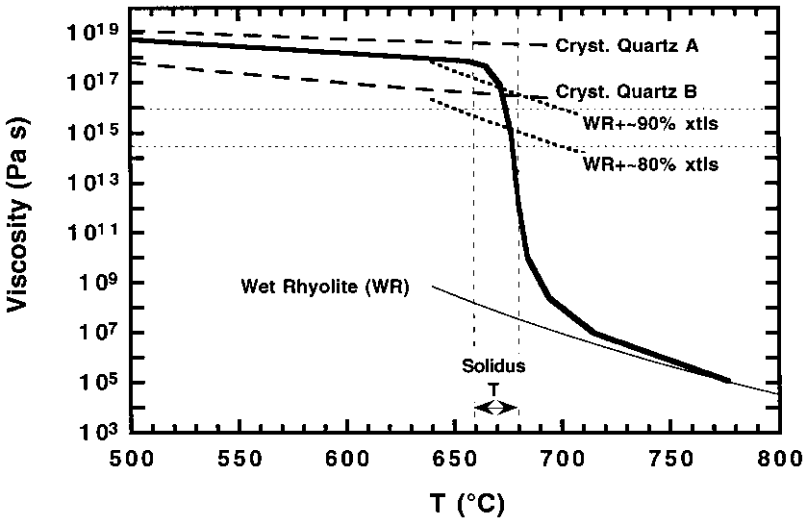

Fig. 9. Viscosity versus temperature for molten rhyolite (light solid curve, Wet Rhyolite), partially crystallized wet rhyolites (light solid curve, WR + xtls) and quartz-rich country rock (dashed curves). Wet rhyolite curve assumes 5 wt% H_2O and is calculated by reducing the viscosity of dry rhyolite (Neuville et al., 1993) by 7 log units (Richet et al., 1996; Schulze et al., 1996). Curves for mostly crystallized rhyolite include melt plus ~80 vol% crystals (wet rhyolite + 7.5 log units) and melt plus ~90 vol% crystals (wet rhyolite + 9 log units) (Lejeune and Richet, 1995; Arzi, 1978a,b; van der Molen and Paterson, 1979). Dashed curves (top) represent effective viscosity of quartz-rich country rock (Ivins, 2000) assuming a constant strain rate of 10^{-13} s^{-1} for (A) "gel" or wet quartz experiments of Patterson and Luan (1990) and Luan and Patterson (1992) and (B) wet Heavitree quartzite (Jaoul et al., 1984). Heavy solid line represents hypothetical viscosity path for a cooling and crystallizing rhyolitic melt, showing slow increase in viscosity as system cools to ~700°C and crystallizes up to ~40%, sharp increase in viscosity as system continues to cool and crystallizes ~40–70%, and continued increase in viscosity as system solidifies at solidus, (vertical dashed lines at 670 ± 10°C), subsequently following crystalline quartz behavior. Horizontal dotted lines indicate viscosity range inferred from shell model and characteristic deformation time for $R_2/R_1 = 1.5$–3.0.

Jaoul et al. (1984), Patterson and Luan (1990) and Luan and Patterson (1992), Ivins (2000) estimated an effective viscosity for wet crystalline quartz of about 10^{17}–10^{19} Pa s at temperatures of 500–600°C, assuming a moderately high strain rate of 10^{-13} s^{-1} (Fig. 9). This viscosity range is somewhat higher than that inferred from our model. However, the model shell assumes a single viscosity value (10^{16} Pa s) that may actually represent an average of a range of values, for example partly molten rhyolite (10^{14} Pa s) and cooler quartz-bearing country rock (10^{18} Pa s).

In summary, largely crystallized rhyolite at or near its solidus temperature (670°C) near the top of the magma chamber (viscosity 10^{15}–10^{17} Pa s) or quartz-bearing crystalline country rock around the magma chamber heated to ~500–600°C (effective viscosity 10^{17}–10^{19} Pa s), are broadly similar to values inferred from a simple viscoelastic shell model and characteristic times for surface deformation data of 34–83 days (~3×10^{14}–10^{16} Pa s). Most of the model runs described below assume a shell viscosity of 10^{16} Pa s, intermediate between this range of values.

3.3.2. Effect of the free surface

One shortcoming of the analytical version of the viscoelastic shell model formulated above is that the elastic medium is assumed to be infinite, i.e. the free surface is not taken into account. However, if we wish to make quantitative comparisons to surface deformation data, it is important to account for the effect of the free surface, across which no stress is transmitted. We have done this with a finite element approach, using the commercial finite element code "ABAQUS" (Hibbit, Karlsson and Sorenson, Inc., 1998). To simplify the calculations, we assumed radial symmetry, and restricted our investigations to a small (500 m radius) spherical pressure source, similar to the Mogi point-source approximation. Thus we do not account

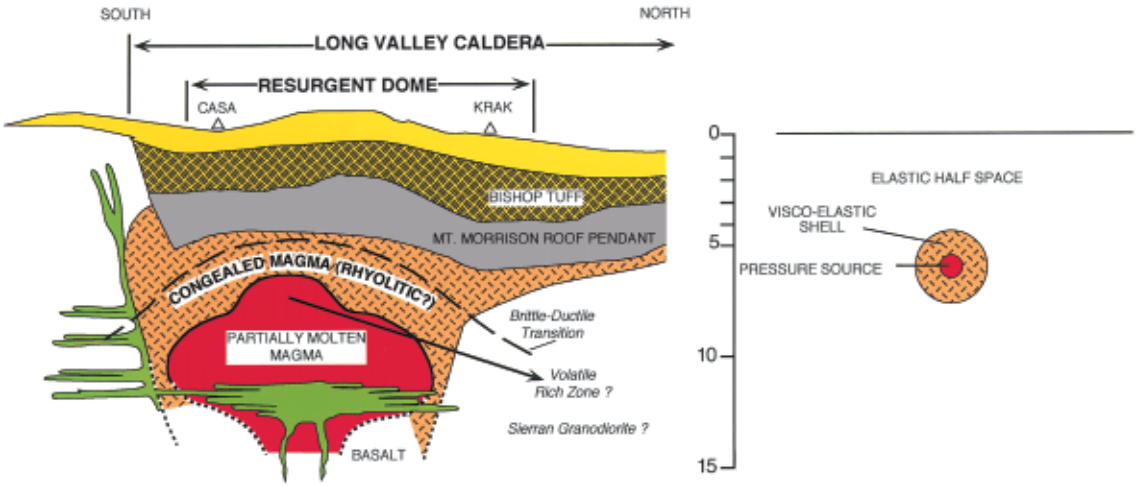

Fig. 10. Left side: hypothetical north–south cross-section for Long Valley Caldera, modified from Hill et al. (1998), showing location of CASA and KRAK, a possible outline of magma chamber and brittle–ductile transition depth. Right side: approximation of this cross-section using a viscoelastic shell model, at the same scale. No vertical exaggeration, scale in km.

for the full spatial complexity of deformation sources at Long Valley (Langbein et al., 1995). We have also ignored topography (flat earth approximation is used) and fixed the depth of the pressure source to 6 km. Fig. 10 diagrams the model geometry and compares it to a more realistic geologic cross-section, modified from Hill et al. (1998). For most of our numerical runs the radius of the shell is 1.5 km (i.e. shell thickness is 1.0 km, $R_2/R_1 = 3.0$).

To check our finite element formulation, we

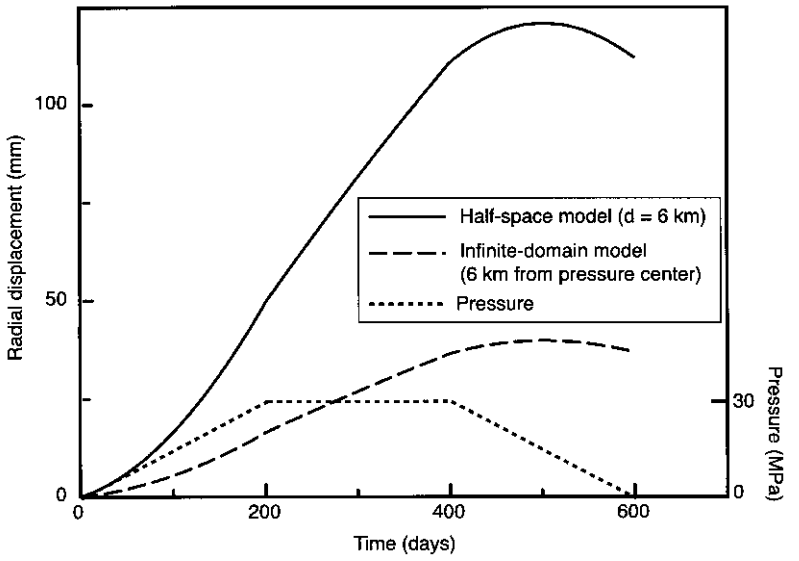

Fig. 11. Predicted surface deformation for the viscoelastic shell model, 6 km from pressure source with trapezoidal time variation of pressure, calculated in two ways: Infinite domain model (elastic full space analytical solution from Dragoni and Magnanensi, 1989), and half space model estimated by finite element technique (this study). The factor of three difference in the predicted amplitudes of the two models represents the effect of the free surface.

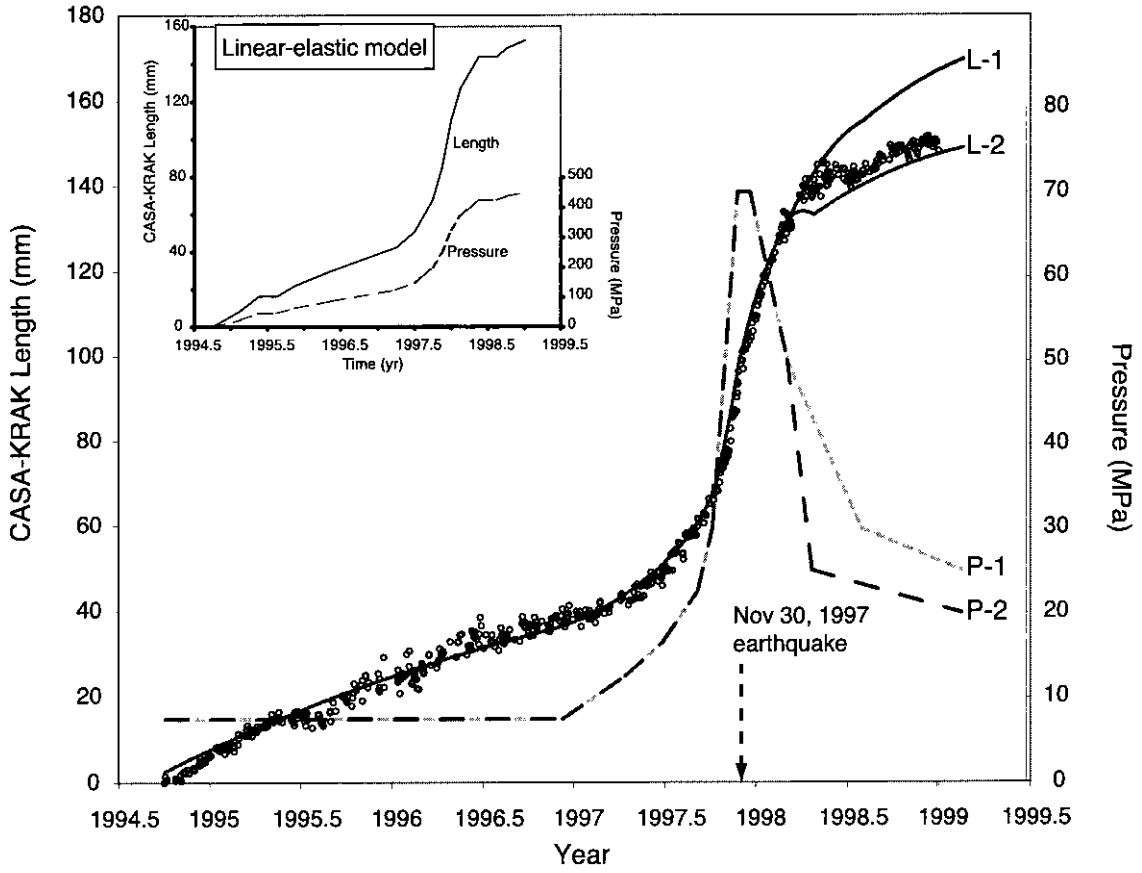

Fig. 12. Observed length (two-color EDM) between CASA and KRAK minus an arbitrary constant (small open circles) between late 1994 and early 1999, compared to predicted length (solid lines, L-1 and L-2) from a viscoelastic shell model calculated by a finite element model approach. Model assumes a spherical source of incremental pressure at 6 km depth and 500 m radius, surrounded by a Maxwell viscoelastic shell 1.0 km thick with viscosity 10^{16} Pa s, embedded in an elastic half space. Light dashed lines (P-1 and P-2) are assumed source pressure history (right-hand scale). Arrow shows time of maximum seismic moment release (November 30, 1997) during this period. Inset shows equivalent purely elastic half space model (i.e. no viscoelastic shell), note higher pressure increments required to match data.

performed two tests. We first set the rheology of the shell to be elastic, obtaining results that are essentially identical to the Mogi point source result (Mogi, 1958). Second, we tested an infinite domain (no free surface) formulation, for comparison to the analytical solution, calculating deformation in the elastic full space 6 km from the center of the pressure source for a simple pressure history. The analytical and finite element results are identical, to better than 0.1 mm/yr (to our knowledge, this is the first numerical test of the analytical viscoelastic shell model of Dragoni and Magnanensi (1989)). Finally, we imposed a free surface on the finite element formulation of the shell model, and performed a series of runs for comparison to the deformation data and to the analytical solution. In one run with a simple pressure history for which the corresponding full space analytical solution is available, the surface deformation patterns are very similar, but the half space solution has three times the amplitude (Fig. 11). In other words, for the tested conditions and at a given distance from the source, a given surface deformation can be obtained with a pressure increment that is three times smaller if the free surface is present compared to the full space solution. This is a very useful result, because it suggests that even though the analytical solution does not account for

the free surface, it can be used to explore the influence of various model parameters without paying the computational cost of the finite element approach, at least within or near the range of conditions tested here.

Fig. 12 shows the surface deformation measured by the two-color EDM on the CASA–KRAK baseline for the 4.5-year period from late 1994 to early 1999, compared to predicted deformation from the viscoelastic shell model, implemented with the finite element formulation (i.e. the free surface is taken into account) and the corresponding pressure history. We use the two-color EDM data here because it is more precise than the GPS data, particularly for short time-scale deformation events, and thus provides a more rigorous test of the model.

In addition to the excellent agreement between model and data, several other features in Fig. 12 are noteworthy:

(1) Prior to the high deformation rate event of mid–late 1997, the pressure increment required to match the data is relatively small and constant.

(2) Prior to early 1997, the deformation rate is slowly decreasing. This is a consequence of viscous relaxation in the shell, perhaps representing a longer term decline from a previous deformation episode.

(3) The entire deformation episode of mid-1997 to early 1998 can be explained by a simple pressure "pulse", in which pressure rises from background values, reaches a peak, and then declines.

(4) Pressure started to increase by December 1996, several months prior to the time when anomalous surface deformation is reliably detected, around April–May 1997 for the two-color EDM, or May–June 1997 for the GPS. This reflects the lag time imposed by the viscous response of the shell, the initially slow rate of pressure increase, and data noise.

(5) Although we have modeled the pressure history as piecewise linear, it is clear that in the early, rising phase of deformation, an exponential-like growth in pressure is required to match the data. This suggests that the observed exponential surface deformation reflects not only the influence of the viscoelastic shell, but also an exponential growth of pressure in the source.

(6) The peak pressures reached are relatively small, less than one half lithostatic pressure, and are maintained for a very short time, a few months or less. The exact value of peak pressure estimated by the model will depend on the size of the source, the size and viscosity of the shell, and the value of rigidity assigned to the elastic and viscoelastic media, reflecting the tradeoff between rheology and source characteristics.

(7) The cessation of pressure buildup coincides with the timing of major seismic moment release from mid–late November 1997 to early December 1997.

(8) A short duration but significant decrease in surface deformation rate occurred in mid-1998. By inspection of pressure curve P-2, it is apparent that this feature can be matched in the model simply by a rapid decrease in pressure to nearly the background value. A simple pressure history intermediate between P-1 and P-2 in Fig. 12 can match the complicated pattern of surface deformation observed in mid-1998 almost exactly.

Fig. 12 (inset) also shows the predicted deformation and corresponding pressure history for a purely elastic half space model, with the same parameters as the shell model (source radius = 500 m, depth = 6 km, rigidity = 5×10^9 Pa) except that shell rheology is set to that of the half space. The fit of model to data is equally good compared to the viscoelastic shell model, however, the peak pressure required to match the data (~500 MPa) is much higher for the purely elastic model than for the shell model (~70 MPa). This exceeds the lithostatic pressure at 6 km (~160 MPa) and thus is unrealistic. The peak pressure required in the purely elastic model could be reduced by using lower values of rigidity or larger values of source radius. Also, in purely elastic models it is possible to define source effects in terms of volume increments rather than pressure increments, thereby avoiding unrealistically high pressures. The volume increment approach may be associated with permanent volume growth of the resurgent dome via magma addition, because after a certain period of time magma loss becomes unlikely due to cooling and solidification (only future observations can indicate whether such growth has actually occurred; significant future subsidence, beyond that expected from thermal contraction of solidifying magma, would tend to rule this out). Thus the high peak pressures indicated in Fig. 12 (inset) for the purely elastic model by themselves do not preclude consideration of such rheology. Nevertheless, it is clear that for equivalent

source characteristics, the viscoelastic shell model can generate the observed deformation with considerably smaller, and thus more physically plausible, pressure increments compared to purely elastic models.

A sensitivity analysis for all of the parameters in the viscoelastic shell model has not been performed; we hope to address this in future studies. For the tested conditions ($R_2/R_1 = 3$), acceptable fits to the data can be obtained with shell viscosities between about 5×10^{15} and 2×10^{16} Pa s. As noted above this range of viscosities is plausible given what we know about the petrology and rheology of the magmatic system at Long Valley and its surroundings.

4. Discussion

4.1. Elastic versus viscoelastic models

Elastic half space models for volcano deformation are often justified on the basis that they fit available data. However this is not always strictly true. Such models may fit surface deformation data, but they often fail to account for other available data on subsurface composition, thermal structure and rheology. The known mineralogy and petrology of crustal materials, laboratory data on the strength of such materials as a function of temperature, and thermal data that constrain the local depth of the transition from brittle behavior, where elastic models are justified, to ductile behavior, where they may not be, all constitute major constraints that need to be incorporated into volcano deformation models. This is especially true for long-lived magmatic/deformation episodes in continental terrains and silicic volcanoes, where magma has time to heat its surroundings, where the ubiquitous presence of quartz means that typical crust enters the ductile deformation field at relatively low temperatures, and where the deformation time scale is sufficiently long to observe viscous behavior. Elastic models are more likely to be good approximations on basaltic shield volcanoes such as Hawaii and Iceland, where quartz is rare or absent, and for short-lived magmatic/deformation episodes, a few days or less, where heating times can be neglected and where the elastic response of typical crustal material likely dominates the viscous response.

The type of geodetic data that we seek to model may also determine whether elastic or viscoelastic models are appropriate. Strainmeters and tiltmeters make precise measurements of strain and tilt on time scales of seconds to days (e.g. Linde et al., 1994). These time scales are short compared to the viscoelastic relaxation time of many materials of geologic interest, hence the elastic approximation is valid. In contrast, displacement methods such as leveling, EDM, GPS or interferomeric SAR are capable of recording long term motions over months or years. These time scales may require incorporation of viscoelastic behavior in the rheological model for the volcano in order to make accurate predictions concerning processes at depth.

In summary, for Long Valley caldera, a long-lived silicic volcanic center in continental crust where leveling, EDM and GPS data record deformation episodes lasting many months or years, incorporating viscoelastic behavior into our rheological models may be important when we seek to relate surface deformation to magmatic processes at depth.

4.2. Pressure variation and implications for magmatic processes

The time history of pressure variation that we infer from our finite element implementation of the viscoelastic shell model, a fairly rapid pressure increase followed by a slower decay, is critical to matching the surface deformation data (Fig. 12). The viscoelastic properties of the shell in our simple model, while contributing to the character of surface deformation, by themselves do not generate exponential surface deformation for simple linear pressure histories (e.g. linear increase followed by linear decrease). Thus the observed surface deformation seems to require an exponential process at depth.

The inferred pressure history gives some clues to the underlying causes of the deformation episode at Long Valley in mid- and late 1997. We suspect that the pressure history is related to intrusion of basaltic magma at the base of the magma chamber and subsequent mixing and heating. Perhaps the pressure pulse is related to a convective overturn event within the magma chamber, associated with earlier or ongoing basaltic intrusion. Intrusion of new basaltic magma or a subsequent overturn event may contribute to rising pressure near the top of the magma chamber in at least three ways: increased

magmatic volume at shallow levels, thermal expansion of heated surroundings, and exsolution of magmatic gas as saturated magma moves upward to lower pressures (the solubility of volatiles in basaltic magma, especially CO_2, is a strong function of pressure in this depth range (Dixon and Stolper, 1995), thus significant degassing is expected).

Magma and fluid volatiles are more likely to be forcibly injected into surrounding country rock near the time of peak pressure, providing a physically plausible mechanism for subsequent pressure drop in the source, and potentially causing: (1) expansion of nearby dikes; (2) slip on nearby faults due to fluid injection and consequent reduction of effective normal stress; and (3) enhanced expulsion of magmatic volatiles. The linear spatial trend of seismicity that we observe near the south moat in November 1997 is consistent with (1) or (2). Dreger et al. (2000) note that four of these earthquakes with $M > 4$ had significant non-double couple components indicating volumetric expansion, also consistent with (1) or (2). McGee et al. (2000) note increased CO_2 flux in September–October 1997 into the gas reservoir near Mammoth Mountain (Farrar et al., 1995; Gerlach et al., 1998), consistent with (3).

The elevated pressure at the top of the magma chamber reached a maximum value in late November 1997, coinciding with the time of maximum seismic moment release (Fig. 12). One scenario consistent with this timing is that pressure in or near the top of the magma chamber increased due to magma rise, stressing adjacent rock until brittle failure conditions were reached somewhere nearby, and/or promoting injection of fluids into pre-existing faults, lowering effective normal stress and leading to large earthquakes. The resulting shaking and rock fracture may have facilitated loss of volatiles from the pressurized magma chamber, and/or intrusion of magma into the country rock, consequently pressure began to decline rapidly. Thus the rapid losses of pressure that we infer to have occurred in December 1997 and early 1998 (Fig. 12) may represent periods of significant fracture opening.

By mid-1999, pressure had declined to a relatively low value, nearly the pre-deformation episode value. Note that with the viscoelastic shell model, rapid uplift continues for several months after pressure begins to decline from its peak value, and the elevated state is maintained for many months, even after pressure has declined to near background values. In contrast, with purely elastic models, the pressure increment must remain at elevated values to maintain the uplifted state (Fig. 12, inset). For long-lived, sustained uplift such as currently characterizes the resurgent dome at Long Valley, this may require maintaining pressure increments approaching lithostatic values for extended periods of time (Bonafede et al., 1986). The pressure variation predicted by the viscoelastic shell model is more physically plausible because peak pressures are only maintained for a short time.

5. Conclusions

Surface deformation at Long Valley increased exponentially in mid- and late 1997 with a time constant of about 60 days, followed by an exponential decrease with about the same time constant. We explain this behavior with a model that incorporates realistic rheology, whereby surface deformation on the resurgent dome mainly reflects an exponential-like pressure increase near the top of the magma chamber, filtered by the viscoelastic response of a ductile, semi-solid rhyolitic "cap" near the top of the magma chamber and/or quartz-bearing country rock surrounding the magma chamber. The pressure increase occurred over about one year, reaching peak values at the end of November 1997, the time of major seismic moment release, after which it declined. Models that incorporate viscoelastic behavior near the magma chamber are preferred over purely elastic models for silicic volcanic centers like Long Valley, particularly for geodetic data spanning several months to years and recording long-lived deformation episodes, where viscous relaxation may be important.

No eruption resulted from the high deformation rate "event" of mid–late 1997, although one can imagine a scenario involving higher surface deformation rates, higher intrusion rates, and higher peak pressures at the top of the magma chamber, culminating in eruption. Perhaps the most important result from the observations described here is that continuous geodetic and seismic monitoring may provide several months warning for this class of volcanic hazard at silicic calderas, as well as providing some constraints on physical properties near the magma chamber.

Acknowledgements

We thank John Langbein for sharing unpublished two-color EDM data, and the Northern California Seismic network, supported by the US Geological Survey, Menlo Park and the Seismological Laboratory, UC Berkeley for earthquake data. We also thank Maurizio Bonafede, Michelle Dragoni, Don Dingwell, Paul Wallace, Anke Freidrich, Dave Jackson, Paul Segall and Eric Ivins for discussions, Bob Tilling for encouragement and Dave Hill for constructive reviews. Several figures in this paper were produced with GMT software (Wessel and Smith, 1995). This work was supported by grants from NASA's Solid Earth and Natural Hazards Program to T. Dixon and NSF grants OCE-9702795 to J. Dixon and EAR-9615561 to T. Dixon.

References

Anderson Jr, A.T., Newman, S., Williams, S.N., Druitt, T.H., Skirius, C., Stolper, E., 1989. H_2O, CO_2, Cl, and gas in Plinian and ash-flow Bishop rhyolite. Geology 17, 221–225.

Arzi, A.A., 1978a. Critical phenomena in the rheology of partially melted rocks. Tectonophysics 44, 173–184.

Arzi, A.A., 1978b. Fusion kinetics, water pressure, water diffusion and electrical conductivity in melting rock, interrelated. J. Petrol. 19, 154–169.

Bailey, R.A., 1984. Chemical evolution and current state of the Long Valley magma chamber. U.S. Geol. Surv., OFR 84-939, pp. 24–40.

Bailey, R.A., 1989. Geologic map of the Long Valley Caldera, Mono–Inyo Craters volcanic chain, and vicinity, Eastern California. Map I-1933, U.S. Geol. Surv. Misc. Invest. Series.

Bailey, R.A., Dalrymple, G.B., Lanphere, M.A., 1976. Volcanism, structure and geochronology of Long Valley Caldera, Mono County, California. J. Geophys. Res. 81, 725–744.

Battaglia, M., Roberts, C., Segall, P., 1999. Magma intrusion beneath Long Valley caldera confirmed by temporal changes in gravity. Science 285, 2119–2122.

Brace, W.F., Kohlstedt, D.L., 1980. Limits on lithospheric stress imposed by laboratory experiments. J. Geophys. Res. 85, 6248–6252.

Bonafede, M., Dragoni, M., Quareni, F., 1986. Displacement and stress fields produced by a centre of dilation and by a pressure source in a viscoelastic half-space: application to the study of ground deformation and seismic activity at Campi Flegrei, Italy. Geophys. J. R. Astron. Soc. 87, 455–485.

Christiansen, R.L., Lipman, P.W., 1972. Cenozoic volcanism and plate tectonic evolution of the western US, 2: Late Cenozoic. Philos. Trans. R. Soc. London Ser. A 271, 249–284.

Cousens, B.L., 1996. Magmatic evolution of Quaternary mafic magmas at Long Valley Caldera and the Devil's Postpile, California: effects of crustal contamination on lithospheric mantle-derived magmas. J. Geophys. Res. 101, 27673–27689.

Dingwell, D.B., 1995. Relaxation in silicate melts: some applications. Mineral. Soc. Am. Rev. Mineral. 32, 21–66.

Dingwell, D.B., Webb, S.L., 1989. Structural relaxation in silicate melts and non-Newtonian melt rheology in geologic processes. Phys. Chem. Minerals 16, 508–516.

Dixon, J.E., Stolper, E.M., 1995. An experimental study of water and carbon dioxide solubilities in mid-ocean ridge basaltic liquids, part II: applications to degassing. J. Petrol. 36, 1633–1646.

Dixon, T.H., Mao, A., Bursik, M., Heflin, M., Langbein, J., Stein, R., Webb, F., 1997. Continuous monitoring of surface deformation at Long Valley Caldera, California, with GPS. J. Geophys. Res. 102, 12017–12034.

Dixon, T.H., Miller, M., Farina, F., Wang, H., Johnson, D., 2000. Present-day motion of the Sierra Nevada block and some tectonic implications for the Basin and Range province, North America Cordillera. Tectonics 19, 1–24.

Dragoni, M., Magnanensi, C., 1989. Displacement and stress produced by a pressurized, spherical magma chamber, surrounded by a viscoelastic shell. Phys. Earth Planet. Inter. 56, 316–328.

Dreger, D.S., Tkalcic, H., Johnston, M., 2000. Dilational processes accompanying earthquakes in the Long Valley Caldera. Science 288, 122–125.

Dunbar, N.W., Hervig, R.L., 1992. Petrogenesis and volatile stratigraphy of the Bishop Tuff: evidence from melt inclusion analysis. J. Geophys. Res. 97, 15129–15150.

Dvorak, J.J., Dzurisin, D., 1997. Volcano geodesy: the search for magma reservoirs and the formation of eruptive vents. Rev. Geophys. 35, 343–384.

Dvorak, J., Okamura, A.T., 1987. A hydraulic model applied to variations in tilt rate during summit subsidence events at Hawaiian volcanoes. In: Decker, R.W., Wright, T.L., Stauffer, P.H. (Eds.), Volcanism in Hawaii vol. 2. US Geol. Surv. Prof Pap. 1350, pp. 1281–1296.

Farrar, C.D., Sorey, M.L., Evans, W.C., Howle, J.F., Kerr, B.D., Kennedy, B.M., 1995. Forest-killing diffuse CO_2 emission at Mammoth Mountain as a sign of magmatic unrest. Nature 376, 675–678.

Eichelburger, J.C., Gooley, R., 1977. Evolution of silicic magma chambers and their relationship to basaltic volcanism. In: Heacock, J.G. (Ed.), The Earth's Crust — Its Nature and Physical Properties. Geophysics Monograph Series, vol. 20. American Geophysical Union, Washington, DC, pp. 57–77.

Eichelburger, J.C., Vogel, T.A., Younker, L.W., Miller, C.D., Keiken, G.H., Wohletz, K.H., 1988. Structure and stratigraphy beneath a young phreatic vent: south Inyo Crater, Long Valley caldera, California. J. Geophys. Res. 93, 13208–13220.

Ferry, J.M., 1996. Three novel isograds in metamorphosed siliceous dolomites from the Ballachulish aureole, Scotland. Am. Mineral. 81, 485–494.

Fink, J.H., 1985. The geometry of silicic dikes beneath the Inyo Domes. J. Geophys. Res 90, 11127–11134.

Gerlach, T.M., Doukas, M.P., McGee, K.A., Kessler, R., 1998. Three year decline of magmatic CO_2 emissions from soils of

a Mammoth Mountain tree kill: Horseshoe Lake, CA, 1995–1997. Geophys. Res. Lett. 25, 1947–1950.

Hanks, T.C., Kanamori, H., 1979. A moment–magnitude scale. J. Geophys. Res. 84, 2348–2350.

Hibbit, Karlsson, Sorenson, Inc., 1998. ABAQUS User's Manual, version 5.8, Hibbit, Karlsson and Sorenson, Inc., Pawtucket, Rhode Island.

Hildreth, W., 1981. Gradients in silicic magma chambers: implications for lithospheric magmatism. J. Geophys. Res. 86, 10153–10192.

Hildreth, W., Mahood, G.A., 1986. Ring fracture eruption of the Bishop tuff. Geol. Soc. Am. Bull. 97, 396–403.

Hill, D.P., Johnston, M.J.S., Langbein, J.O., McNutt, S.R., Miller, C.D., Mortensen, C.E., Pitt, A.M., Rojstaczer, S., 1991. Response plans for volcanic hazards in the Long Valley Caldera and Mono Craters area, California. U.S. Geol. Surv. OFR 91-270.

Hill, D.P., Ellsworth, W.L., Johnston, M.J.S., Langbein, J.O., Oppenheimer, D.H., Pitt, A.M., Reasenberg, P.A., Sorey, M.L., McNutt, S.R., 1990. The 1989 Earthquake swarm beneath Mammoth Mountain, California: An Initial Look at the 4 May through 30 September Activity. Bull. Seismol. Soc. Am. 80, 325–339.

Hill, D.P., Sorey, M.L., Ellsworth, W.L., 1998. Scientific drilling continues in Long Valley Caldera, California. EOS, Trans. Am. Geophys. Union 79, 429.

Hill, D.P., 1992. Temperatures at the base of the seismogenic crust beneath Long Valley Caldera, California, and the Phlegrean Fields Caldera, Italy. In: Gasparini, P., Scarpa, R., Aki, K. (Eds.), Volcanic Seismology. IAVCEI Proceedings in Volcanology, vol. 3. Springer, Berlin, pp. 432–461.

Ivins, E.R., 2000. Correction to Transient creep of a composite lower crust 2. A polymineralic basis for rapidly evolving post-seismic deformation modes. J. Geophys. Res. 105, 3229–3232.

Izett, G.A., Obradovitch, J.D., 1994. 40Ar–39Ar age constraints for the Jaramillo normal subchron and the Matuyama–Brunhes geomagnetic boundary. J. Geophys. Res. 99, 2925–2934.

Jaoul, O., Tullis, J., Kronenburg, A., 1984. The effect of varying water contents on the creep behavior of Heavitree quartzite. J. Geophys. Res. 89, 4298–4312.

Johnston, D.A., 1978. Volatiles, magma mixing, and the mechanism of eruption of Augustine volcano, Alaska. PhD thesis, University of Washington, Seattle, WA.

Kenner, S.J., Segall, P., 2000. Post-seismic deformation following the 1906 San Francisco earthquake. J. Geophys. Res. 105, 13195–13210.

Kirby, S.H., Kronenburg, A.K., 1987. Rheology of the lithosphere: selected topics. Rev. Geophys. Space Phys. 25, 1219–1244.

Langbein, J.O., 1989. Deformation of the Long Valley Caldera, eastern California, from mid-1983 to mid-1988: measurements using a two color geodimeter. J. Geophys. Res. 94, 3833–3849.

Langbein, J.O., Hill, D.P., Parker, T.N., Wilkinson, S.K., 1993. An episode of re-inflation of the Long Valley Caldera, eastern California, 1989–1991. J. Geophys. Res. 98, 15851–15870.

Langbein, J.O., Dzurisin, D., Marshall, G., Stein, R., Rundle, J., 1995. Shallow and peripheral volcanic sources of inflation revealed by modeling two-color geodimeter and leveling data from Long Valley caldera, California, 1988–1992. J. Geophys. Res. 100, 12487–12495.

Langbein, J., Wilkinson, S., Johnston, M., Feinberg, J., Bilham, R., 1998. The 1997–98 inflation episode of Long Valley caldera and comparison with the 1989–95 episode. EOS: Trans. Am. Geophys. Union 79 (45), F963.

Lejeune, A.-M., Richet, P., 1995. Rheology of crystal-bearing silicate melts: an experimental study at high viscosities. J. Geophys. Res. 100, 4215–4229.

Linde, A., Agustssin, K., Sacks, I.S., Stefansson, R., 1994. Mechanism of the 1991 eruption of Hekla from continuous borehole strain monitoring. Nature 365, 737–740.

Luan, F.C., Patterson, M.S., 1992. Preparation and deformation of synthetic aggregates of quartz. J. Geophys. Res. 97, 301–320.

Maaløe, S., Wyllie, P., 1975. Water content of a granite magma deduced from the sequence of crystallization determined experimentally with water-undersaturated conditions. Contrib. Mineral. Petrol. 52, 175–191.

Mankinen, E.A., Gromme, M.C.S., Dalyrymple, G.B., Lanphere, M.A., Bailey, R.A., 1986. Paleomagnetism and K–Ar ages of volcanic rocks from Long Valley Caldera, California. J. Geophys. Res. 91, 633–652.

Marchildon, N., Dipple, G.M., 1998. Irregular isograds, reaction instabilities and the evolution of permeabiliy during metamorphism. Geology 26, 15–18.

Marsh, B.D., 1981. On the crystallinity, probability of occurrence, and rheology of lava and magma. Contrib. Mineral. Petrol. 78, 85–98.

Mao, A., Harrison, C.G., Dixon, T.H., 1999. Noise in GPS coordinate time series. J. Geophys. Res 104, 2797–2816.

McGee, K.A., Gerlach, T.M., Kessler, R., Douglas, M.P., 2000. Geochemical evidence for a magmatic CO_2 degassing event at Mammoth Mountain, California, September–December 1997. J. Geophys. Res. 105, 8447–8456.

Metz, J.M., Mahood, G.A., 1985. Precursors to the Bishop Tuff eruption: Glass Mountain, Long Valley, California. J. Geophys. Res. 90, 11121–11126.

Miller, C.D., 1985. Holocene eruptions at the Inyo volcanic chain, California: implications for possible eruptions in Long Valley Caldera. Geology 13, 14–17.

Mogi, K., 1958. Relations between the eruptions of various volcanoes and the deformations of the ground surfaces around them. Bull. Earthquake Res. Inst., Univ. Tokyo 36, 99–134.

Neuville, D.R., Courial, P., Dingwell, D.B., Richet, P., 1993. Thermodynamic and rheological properties of rhyolite and andesite melts. Contrib. Mineral. Petrol. 113, 572–581.

Newman, S., Epstein, S., Stolper, E., 1988. Water carbon dioxide and hydrogen is glasses from the ca. 1340 AD eruption of the Mono Craters, California: constraints on degassing phenomena and initial volatile content. J. Volcanol. Geotherm. Res. 35, 75–96.

Owen, S., Segall, P., Lisowski, M., Miklius, A., Bevis, M., Foster, J., 1997. The January 30, 1997 fissure eruption in Kilauea's East Rift Zone as measured by continuous GPS. EOS, Trans. Am. Geophys. Union 78, S105.

Pallister, J.S., Hoblitt, R.P., Reyes, A.G., 1992. A basalt trigger for the 1991 eruptions of Pinatubo volcano?. Nature 356, 426–428.

Patterson, M.S., Luan, F.C., 1990. Quartzite rheology under geological conditions. In: Knipe, R.J., Rutter, E.H. (Eds.),

Deformation Mechanisms, Rheology and Tectonics. Geol. Soc., London, Spec. Publ. 54. 299–307.

Pollitz, F.F., Peltzer, G., Bürgmann, R., 2000. Mobility of continental mantle: evidence from post-seismic geodetic observations following the 1992 Landers earthquake. J. Geophys. Res. 105, 8035–8054.

Richet, P., Bottinga, Y., 1995. Rheology and configurational entropy of silicate melts. Mineral. Soc. Am. Rev. Mineral. 32, 67–93.

Richet, P., Lejeune, A.-M., Holtz, F., Roux, J., 1996. Water and viscosity of andesite melts. Chem. Geol. 128, 185–197.

Rundle, J., et al., 1985. Seismic imaging in Long Valley, California, by surface and borehole techniques: an investigation of active tectonics. EOS: Trans. Geophys. Union 66, 194–210.

Rundle, J.B., Hill, D.P., 1988. The geophysics of a restless caldera — Long Valley, California. Annu. Rev. Earth Planet. Sci. 16, 251–271.

Sanders, C.O., Nixon, L.D., 1995. S wave attenuation structure in Long Valley caldera, California from three-component S to P amplitude ratio data. J. Geophys. Res. 100, 12395–12404.

Sanders, C.O., Ponko, S.C., Nixon, L.D., Schwartz, E.A., 1995. Seismological evidence for magmatic and hydrothermal structure in Long Valley caldera from local earthquake attenuation and velocity tomography. J. Geophys. Res. 100, 8311–8326.

Savage, J.C., Cockerham, R.S., 1984. Earthquake swarm in Long Valley Caldera, California, January 1983: evidence for dike inflation. J. Geophys. Res. 89, 8315–8324.

Savage, J.C., Cockerham, R.S., Estrem, J.E., Moore, L.R., 1987. Deformation near Long Valley Caldera, Esastern California, 1982–1986. J. Geophys. Res. 92, 2721–2746.

Savage, J.C., Lisowski, M., 1998. Viscoelastic coupling model of the San Andreas fault along the big bend, southern California. J. Geophys. Res. 103, 7281–7292.

Schulze, F., Behrens, H., Holtz, F., Roux, J., Johannes, W., 1996. The influence of H_2O on the viscosity of a haplogranitic melt. Am. Mineral. 81, 1155–1165.

Sieh, K., Bursik, M., 1986. Most recent eruption of the Mono Craters, eastern central California. J. Geophys. Res. 91, 12539–12571.

Sillard, P., Altamimi, Z., Boucher, C., 1998. The ITRF96 realization and its associated velocity field. Geophys. Res. Lett. 25, 3222–3226.

Skirius, C., 1990. Pre-eruptive water and carbon-dioxide content of Plinian and ash-flow Bishop Tuff Magma. PhD thesis, University of Chicago, Chicago, IL.

Sorey, M.L., 1985. Evolution and present state of the hydrothermal system in Long Valley Caldera. J. Geophys. Res. 90, 11219–11229.

Sparks, S.R., Sigurdson, H., Wilson, L., 1977. Magma mixing a mechanism for triggering acid explosive eruptions. Nature 267, 315–318.

Steck, L.K., Prothero, W.A., 1994. Crustal structure beneath Long Valley caldera from modeling of teleseismic P-wave polarizations and Ps converted waves. J. Geophys. Res. 99, 6881–6898.

Stroujkova, A.F., Malin, P.E., 2000. A magma mass beneath Casa Diablo? Further evidence from reflected seismic waves. Bull. Seismol. Soc. Am. 90, 500–511.

Thatcher, W., 1983. Non-linear strain build-up and the earthquake cycle on the San Andreas fault. J. Geophys. Res. 88, 5893–5902.

Trygvason, E., 1980. Subsidence events in the Krafla area, north Iceland, 1975–1979. J. Geophys. Res. 47, 141–153.

van der Molen, I., Paterson, M.S., 1979. Experimental deformation of partially-melted granite. Contrib. Mineral. Petrol. 70, 299–318.

Varga, R.J., Bailey, R.A., Suemnicht, G.A., 1990. Evidence for 600 year old basalt and magma mixing at Inyo Craters volcanic chain, Long Valley Caldera, California. J. Geophys. Res. 95, 21441–21450.

Vogel, T.A., Eichelberger, J.C., Younker, L.W., Schuraytz, B., Horkowitz, J., Stockman, H., Westrich, H., 1989. Petrology and emplacement of intrusive and extrusive rhyolites of Obsidian Dome, Inyo Craters volcanic chain, eastern California. J. Geophys. Res. 94, 17937–17956.

Vogel, T.A., Woodbourne, T.B., Eichelberger, J.C., Layer, P.W., 1994. Chemical evolution and periodic eruption of mafic lava flows in the west moat of Long Valley Caldera, California. J. Geophys. Res. 99, 19829–19842.

Wallace, P.J., Anderson Jr, A.T., Davis, A.M., 1995. Quantification of pre-eruptive exsolved gas contents in silicic magmas. Nature 377, 612–616.

Webb, S.L., Dingwell, D.B., 1995. Viscoelasticity. Mineral. Soc. Am. Rev. Mineral. 32, 95–119.

Wessel, P., Smith, W.H.F., 1995. New version of Generic Mapping Tools. EOS 16, 329.

Winkler, J.G.F., 1974. Petrogenesis of Metamorphic Rocks. Springer, New York, 276 pp.

Zumberge, J.F., Heflin, M., Jefferson, D., Watkins, M., Webb, F., 1997. Precise point positioning for efficient and robust analysis of GPS data. J. Geophys. Res. 102, 5005–5017.